Long-lived pressure-driven coherent structures in KSTAR plasmas

S. G. Lee, J. Seol, H. H. Lee, A. Y. Aydemir, L. Terzolo, K. D. Lee, Y. S. Bae, J. G. Bak, G. H. Choe, G. S. Yun, and J. W. Yoo

Citation: Physics of Plasmas **23**, 052511 (2016); doi: 10.1063/1.4949768
View online: http://dx.doi.org/10.1063/1.4949768
View Table of Contents: http://scitation.aip.org/content/aip/journal/pop/23/5?ver=pdfcov
Published by the AIP Publishing

Long-lived pressure-driven coherent structures in KSTAR plasmas

S. G. Lee,[1,a)] J. Seol,[1] H. H. Lee,[1] A. Y. Aydemir,[1] L. Terzolo,[1] K. D. Lee,[1] Y. S. Bae,[1] J. G. Bak,[1] G. H. Choe,[2] G. S. Yun,[2] and J. W. Yoo[3]
[1]*National Fusion Research Institute, Daejeon, South Korea*
[2]*Pohang University of Science and Technology, Pohang, South Korea*
[3]*Korea University of Science and Technology, Daejeon, South Korea*

(Received 2 March 2016; accepted 2 May 2016; published online 16 May 2016)

Highly coherent structures associated with an extremely long-lived saturated magnetohydrodynamic instability have been observed in KSTAR tokamak under a long-pulse and steady-state operation. They persist essentially unchanged for the full duration of a discharge up to 40 s, much longer than any dynamical or dissipative time scales in the system. Analysis of the data, supported by numerical simulations, indicates that they may be associated with a pressure-driven mode causing some degradation in the toroidal rotation, electron, and ion energy confinement. *Published by AIP Publishing.*
[http://dx.doi.org/10.1063/1.4949768]

I. INTRODUCTION

Understanding coherent structures that persist for very long times on the dynamical and dissipative time scales of a system always presents a challenge. The snakes seen on spatiotemporal plots of soft X-ray signals on rational magnetic surfaces are probably the earliest examples of long-lived structures in laboratory plasmas.[1] Usually, they are attributed to an excess density or impurity concentration trapped in an $m = 1$ magnetic island. More recently, an alternative explanation for snakes has been offered in terms of bifurcated three dimensional equilibria in low or reversed-shear discharges within still axisymmetric boundaries,[2,3] consistent with a saturated quasi-interchange mode.[4–6] Regardless of their actual origin, the snakes seem to defy normal transport processes in their extreme longevity. New observations of the formation and dynamics of long-lived impurity-induced helical snakes have recently investigated on Alcator C-Mod.[7] The measured snakes form as an asymmetry in the impurity ion density with accompanying sawtooth oscillations.

Another experimental observation of long-lived mode has been observed on MAST[8] and HL-2A[9] devices. Neutral beam injection (NBI) heated plasmas in MAST with an advanced tokamak scenario safety factor profile above unity open exhibited long-lived saturated $n = 1$ magnetohydrodynamic (MHD) instabilities.[8] The saturated MHD instability observed on MAST showed an internal kink structure without magnetic islands, and the core toroidal rotation was reduced in the presence of such ideal modes. HL-2A showed similar $n = 1$ long-lived internal modes during NBI heated plasmas when the safety factor profile has a weak shear in a broad range of the plasma center with central safety factor (q_0) around unity. The long-lived internal mode observed on HL-2A showed a pressure-driven feature, and it was successfully suppressed by electron cyclotron heating (ECH) or supersonic molecular beam injection.[9]

We report on the first observation of an extremely long-lived pressure-driven coherent structure in the plasma core of KSTAR, an advanced superconducting tokamak pursuing steady-state and high-performance operating scenarios.[10] As the plasma performance is increased in advanced tokamak regimes, possible deleterious effects of MHD modes become more important, especially for steady-state burning plasmas in the next-step devices such as ITER and DEMO. One of the commonly seen modes is the $m = 2$, $n = 1$ resistive kink (or neoclassical tearing) mode that either leads to confinement degradation, or mode locking followed by a full disruption.[11–13] In KSTAR, however, long-pulse discharges regularly exhibit a coherent structure in the form of a saturated pressure-driven MHD mode that can be sustained as long as 40 s, the full discharge duration, when the mode is located near the plasma core region with a broad safety factor profile with $q_0 \geq 2$.

Similar to MAST plasmas, the central toroidal rotation decreases; during that time, long-lived mode exists in KSTAR. Recently, toroidal rotation is focused as an important topic for the major tokamaks including future burning plasma devices since it is essential for the stabilization of resistive wall modes,[14] and its shear plays an important role to improve plasma confinement by suppressing turbulent transport.[15] A dramatic central toroidal rotation damping during on-axis ECH injection has been related to neoclassical toroidal viscosity caused by the excitation of an internal kink mode in KSTAR plasmas.[16] Although the toroidal rotation reduction due to the long-lived MHD modes in KSTAR plasmas is not severe, it can be sustained for extremely long duration in the steady-state operation. Therefore, understanding of extremely long-lived MHD modes could bring novel insight into steady-state operation capabilities[17–19] for the future burning plasmas.

II. EXPERIMENTAL OBSERVATIONS AND NUMERICAL SIMULATIONS

The KSTAR machine is a medium-size, D-shaped tokamak with the major radius $R = 1.8$ m, minor radius $a = 0.5$ m, and typical toroidal magnetic field is between 2.0 and 3.5 T at the plasma center. In this experiment, all plasma discharges are in deuterium and the toroidal magnetic field is

a)E-mail: sglee@nfri.re.kr

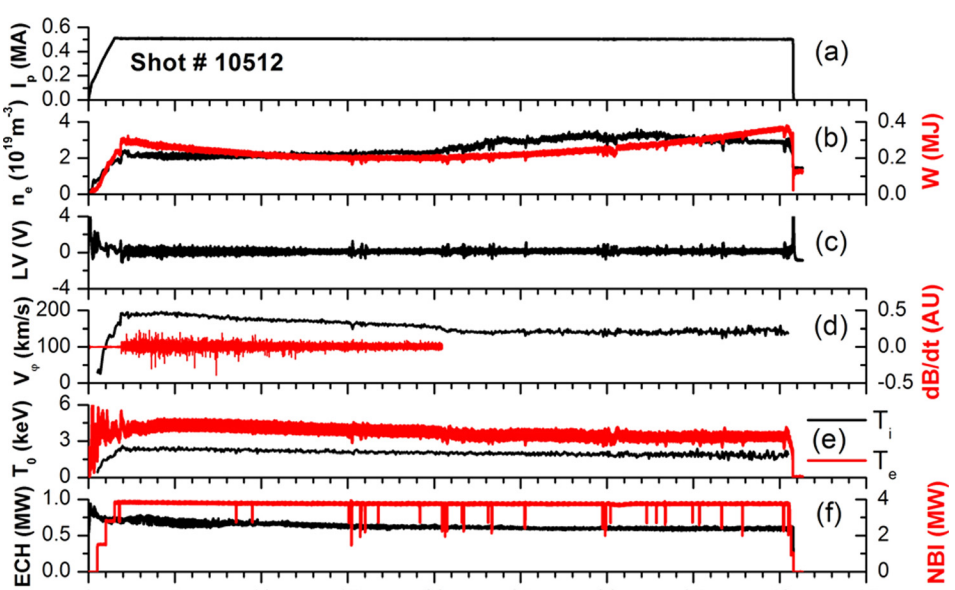

FIG. 1. Time traces of the plasma parameters from long-pulse discharge for shot 10 512. A large coherent T_e oscillation is sustained as long as 40 s. (a) The plasma current. (b) The electron density and total stored energy. (c) The loop voltage. (d) The central toroidal rotation and magnetic fluctuation. (e) The core ion and electron temperatures. (f) The auxiliary heating power from NBI and ECH.

3.0 T. Figure 1 shows time traces of the various plasma parameters for a long-pulse discharge with an advanced tokamak scenario to perform steady-state operation without any sawtooth oscillations. The normalized plasma beta (β_N) is about 1.4 with shaping factors as $\kappa \sim 1.8$ and $\delta \sim 0.6$. As shown in Fig. 1(a), the plasma current (I_p) is 0.5 MA, and it is well controlled for up to 40 s until the discharge is terminated by interlock due to overheating in the divertor since it is not actively cooled. The electron density (n_e) from a single-channel mm-wave interferometer and total stored energy are shown in Fig. 1(b). Note that the electron density and stored energy increasing at about 20 s are induced due to the divertor overheating. The loop voltage shown in Fig. 1(c) is almost zero and essentially constant during the plasma current flat-top region, indicating a significant fraction of non-inductive current drive. The central toroidal rotation (V_φ) from an X-ray imaging crystal spectrometer (XICS)[20] and magnetic fluctuation for the MHD activity measured from a Mirnov coil with good temporal resolution up to 200 kHz are shown in Fig. 1(d). Although the magnetic fluctuation measurement is limited to the first 20 s due to a memory-size limitation, the fluctuations remain for the full duration of the discharge. This long-lived saturated magnetic fluctuation is analysed as a pressure-driven $n = 1$ mode. The details of mode analysis and simulation studies are discussed later. The central ion temperature (T_i) from the XICS and electron temperature (T_e) from an electron cyclotron emission (ECE) are shown in Fig. 1(e). A large coherent T_e oscillation from the ECE shows a similar structure as shown from the Mirnov coil. The T_e oscillation from the ECE can be measured for the full duration of the discharge since the sampling rate of the ECE is set at one-half of the Mirnov coil's sampling rate. In KSTAR plasmas, long-lived saturated magnetic fluctuations like this are seen when an early NBI together with an auxiliary on-axis 170 GHz ECH is applied, as shown in Fig. 1(f). The total heating power of about 4.6 MW is delivered from the NBI (3.8 MW) and ECH (0.8 MW). It seems that the ECH can trigger pressure-driven modes by modifying the pressure profile. In general, the early heating tends to increase T_e and consequently the plasma resistivity decreases, which means the inductively driven current takes longer to diffuse into the core region so that the safety factor profile easily has broad weak shear as shown in Fig. 2 where the safety factor is not directly measured but it is calculated using the TRANSP[21] code. The safety factor profile is also analysed by the EFIT reconstruction code[22] in Fig. 2. Under this safety factor profile condition, the steady-state long-pulse advanced tokamak operation could be accessed more easily. The calculated central safety factor is confirmed above unity since there are no sawtooth oscillations in Fig. 1(e). The calculated safety factor profile in Fig. 2 is used by numerical simulations, and the simulated result of the MHD mode image is verified with that of experimentally measured from an electron cyclotron emission imaging (ECEI) diagnostic,[23] which will be described later. The toroidal rotation, electron, and ion temperatures gradually decrease during the time long-lived saturated magnetic fluctuations exist as shown in Fig. 1. A typical momentum confinement time is

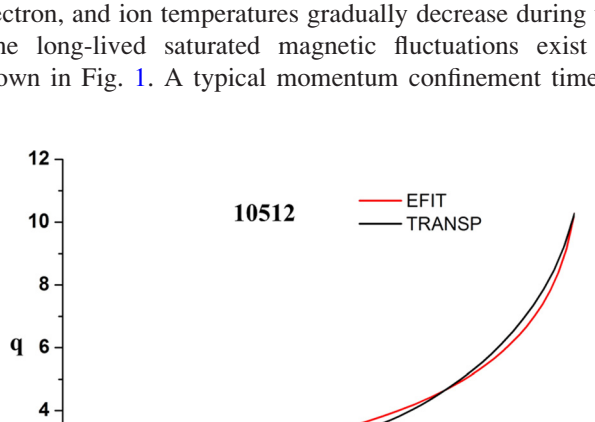

FIG. 2. Safety factor profile calculated from the TRANSP and EFIT code showing a broad weak shear with central safety factor above 2.

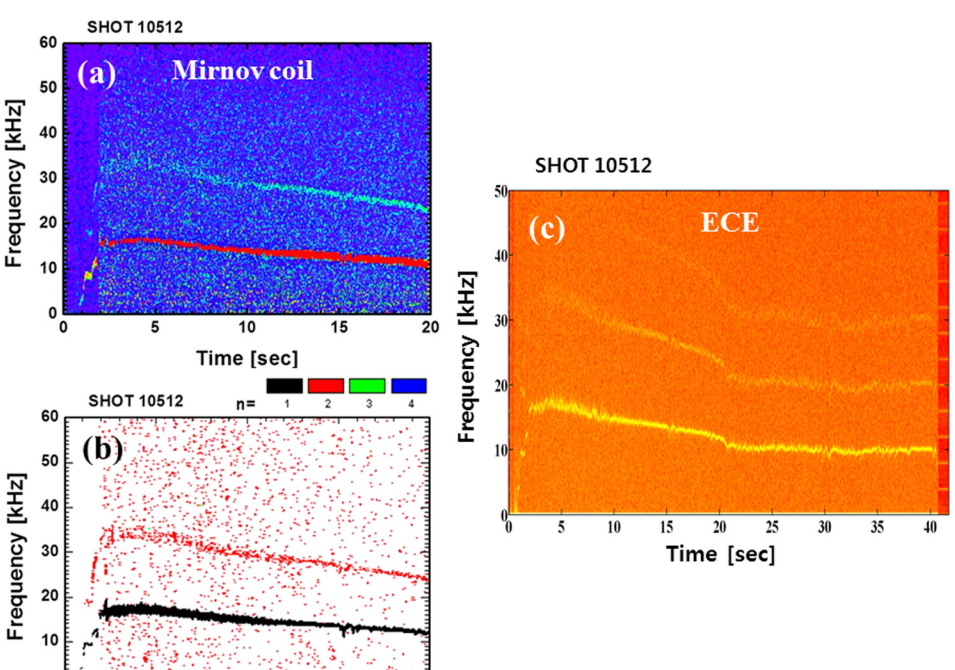

FIG. 3. Time evolution of the frequency spectrum from a fast Fourier transform for the MHD activity shown in Fig. 1. (a) Fourier spectrogram of Mirnov coil measurement. (b) The toroidal mode number spectrogram of Mirnov coil measurement. (c) Fourier spectrogram of ECE measurement.

about 100–150 ms, so that the saturated magnetic fluctuation persists much longer than any dissipative time scale since the discharge sustains up to 40 s. The toroidal rotation measured by XICS has been validated by charge exchange spectroscopy utilizing a two-Gaussian fitting since NBI modulation was not applied in Fig. 1.[24]

The time evolution of the frequency spectrum of the MHD activity measured from the Mirnov coil shown in Fig. 1(d) is analysed by a fast Fourier transform method, and the intensity and mode structure obtained are illustrated in Figs. 3(a) and 3(b), respectively. Figure 3(c) shows the full discharge spectrogram of the T_e oscillation measured by the ECE. The dominant toroidal mode is $n = 1$ and subdominant mode is $n = 2$ at about twice the frequency from the spectrum analyses. The measured core $V_\varphi \cong 200$ km/s, shown in Fig. 1(d), corresponds to a mode with the rotation frequency of $f = 18$ kHz (at major radius $R = 1.8$ m), as follows from the equation: $V_\varphi = 2\pi \cdot R \cdot f$. The frequency f, which is postulated by this equation, is close to the measured frequency of the toroidal mode with mode number $n = 1$ from the Mirnov coil and ECE as shown in Figs. 3(b) and 3(c), respectively. We note that with the strong external momentum input by NBI, the frequencies of the observed MHD modes are found to be consistent with the central toroidal rotation velocity. The diamagnetic rotation in the frequency analysis is not taking into account since its contribution is negligible.

The long-lived saturated magnetic fluctuation disappears when the ECH is turned off at about 32 s as shown another

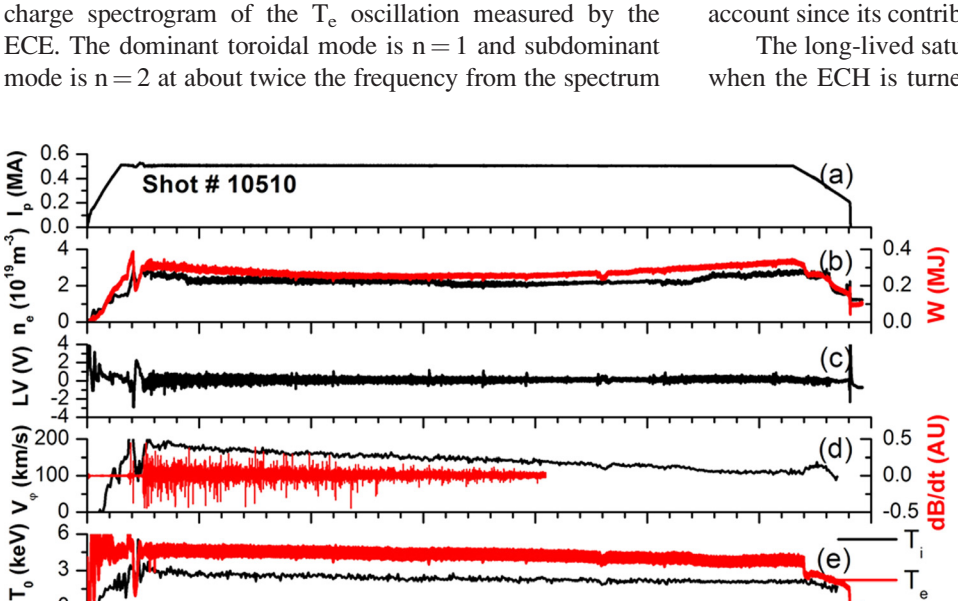

FIG. 4. Time traces of the plasma parameters from long-pulse discharge for shot 10510. The large coherent T_e oscillation is disappeared when the ECH is turned off at about 32 s. (a) The plasma current. (b) The electron density and total stored energy. (c) The loop voltage. (d) The central toroidal rotation and magnetic fluctuation. (e) The core ion and electron temperatures. (f) The auxiliary heating power from NBI and ECH.

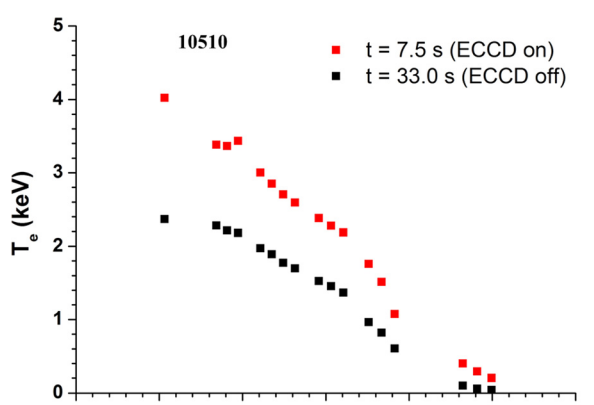

FIG. 5. T_e profiles measured by ECE diagnostic. The electron temperature and temperature gradient increased during ECH injection.

similar discharge in Fig. 4. The central electron temperature and its fluctuations measured from the ECE diagnostic dramatically reduced as soon as the ECH is turned off in Fig. 4(e). At the same time, the core V_φ measured from the XICS recovers as shown in Fig. 4(d). It is noted that the long-lived saturated magnetic fluctuation is measured when on-axis ECH is applied together with early NBI heating during the plasma current ramp-up period, which indicates that it originates from the pressure gradient in plasmas with a safety factor profile having a broad weak induced by ECH injection. The electron temperature profiles with and without ECH for shot 10510 are shown in Figure 5. The electron temperature and temperature gradient in the core region increased a lot during ECH injection. Note that the ECE diagnostic did not have full coverage of the plasma core region due to the higher magnetic field used in this discharge (3.0 T). Figure 6 shows typical plasma parameters under another similar steady-state operation without ECH injection. Under this condition, the long-lived saturated magnetic fluctuation is not generated even if there is early NBI heating during the plasma current ramp-up period since there are no corresponding modes as shown in Figs. 7(a)–7(c), which are analysed in the time evolution of the frequency spectrum of the Mirnov coil and the ECE measurements shown in Fig. 6. Note that shot 10531 shown in Fig. 6 is reproduced under the similar experimental conditions with previous two shots of 10510 and 10512. However, the electron density for shot 10531 is approximately a factor of two higher than that of shots 10510 and 10512. This may cause that the central toroidal rotation for shot 10531 decreases linearly even though there are no long-lived modes existed. If on-axis ECH was injected and the long-lived mode was generated, additional toroidal rotation drop would be expected in shot 10531.

Figure 8 shows a two-dimensional $\delta T_e/\langle T_e\rangle$ ECE image for shot 10512 during the long-lived saturated magnetic fluctuation measured by the ECEI diagnostic. The ECEI is an advanced diagnostic system to visualize MHD instabilities.[25,26] Three images at $\pi/2$ different phases of the measured pressure-driven mode are plotted as it rotates in the clockwise, indicating the poloidal mode number is $m = 2$. Therefore, the long-lived pressure-driven magnetic fluctuation is identified as an $m/n = 2/1$ mode since the $m = 2$ MHD image is clearly observed from Figs. 8(a)–8(c), and the mode is located near the plasma center at $R = 180$ cm. The arrows shown in Fig. 8(a) indicate that the rotational motion of the mode structure is in the poloidal direction. In addition, the measured ECE images shown in Figs. 8(a)–8(c) show a strong ballooning character.

The experimental observation is confirmed by a simulation as follows. We have done nonlinear numerical simulations using the CTD code[27] with the safety factor profile shown in Fig. 2. Even without a $q = 2$ rational surface in the plasma, we find a pressure-driven $n = 1$ mode, predominantly with an $m = 2$ component, at $\beta_N = 1.36$, which is close to experimental values. Synthetic ECEI data in Fig. 9, showing $\delta p/p$, where $\delta p \equiv p - p(n = 0)$, are in remarkably good agreement with the experimental observations by comparing with Fig. 8. Note that

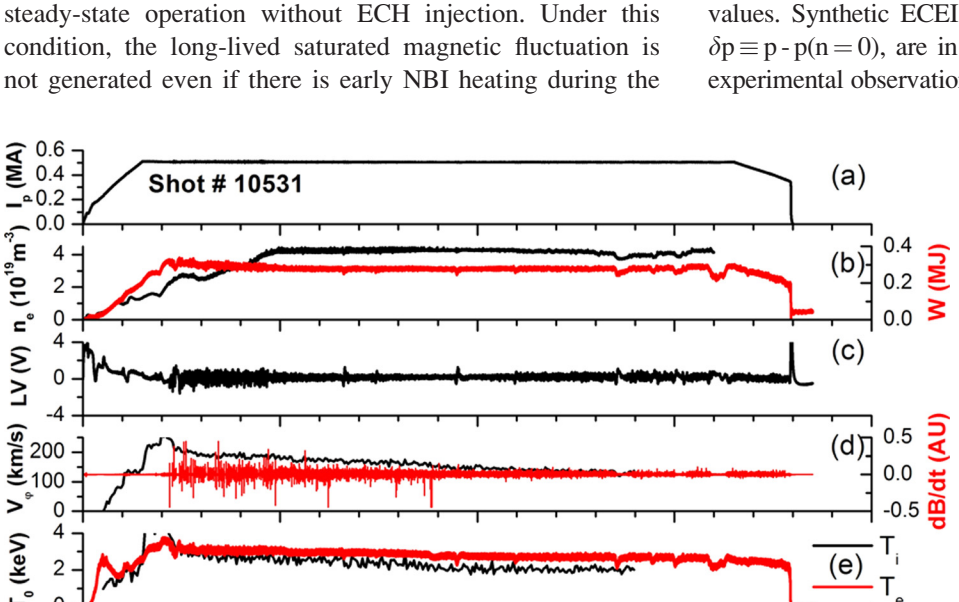

FIG. 6. Time traces of the plasma parameters from long-pulse discharge for shot 10 531. There are no coherent oscillations without ECH injection. (a) The plasma current. (b) The electron density and total stored energy. (c) The loop voltage. (d) The central toroidal rotation and magnetic fluctuation. (e) The core ion and electron temperatures. (f) The auxiliary heating power from only NBI.

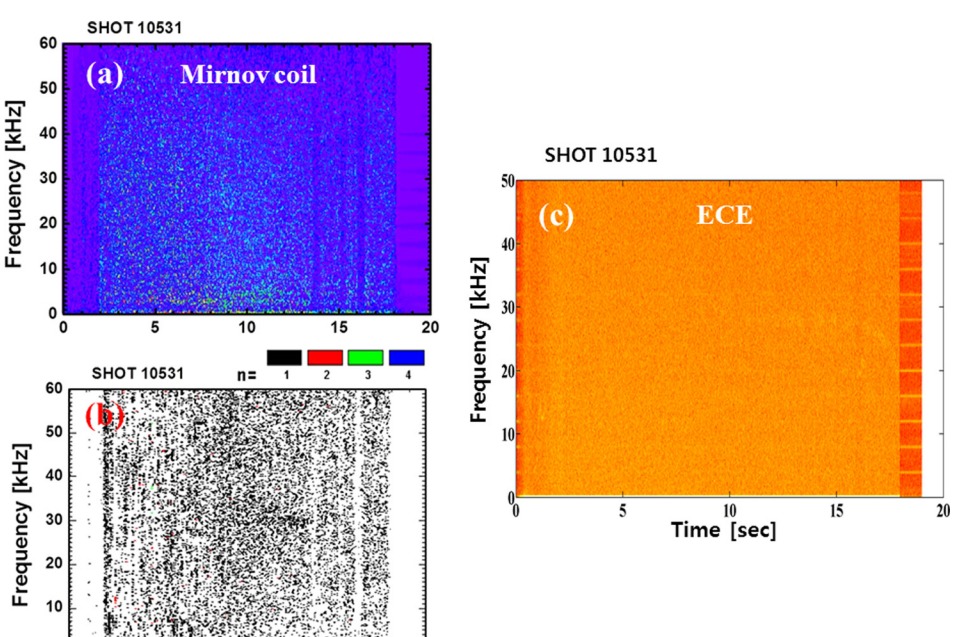

FIG. 7. Time evolution of the frequency spectrum from a fast Fourier transform from the Mirnov coil and ECE measurements shown in Fig. 6. (a) Fourier spectrogram of Mirnov coil measurement. (b) The toroidal mode number spectrogram of Mirnov coil measurement. (c) Fourier spectrogram of ECE measurement.

the nonlinear pressure perturbation δp shows a strong ballooning character, as expected from a kink-ballooning mode. These preliminary calculations done in circular geometry are being extended to shaped profiles; the results will be presented elsewhere.

III. CONCLUSION

Highly coherent structures associated with a saturated extremely long-lived MHD instability have been observed in the superconducting KSTAR tokamak for the first time. They persist essentially unchanged for the full duration of a discharge, much longer than any dynamical or dissipative time scales in the system. The extremely long-lived pressure-driven MHD mode is measured when on-axis ECH is applied together with early NBI heating during the plasma current ramp-up period under the safety factor well above unity. It seems that the ECH can trigger pressure-driven modes by modifying the pressure profile since the electron temperature and temperature gradient in the core region increased substantially during ECH injection. The long-lived pressure-driven MHD mode is further identified as an m/n = 2/1 mode from two-dimensional $\delta T_e/\langle T_e\rangle$ ECE image measured by the ECEI diagnostic and Fourier spectrogram of the Mirnov coil and ECE measurements. The measured ECE image during the time long-lived pressure-driven mode exists showed a strong ballooning character, and it is confirmed by nonlinear numerical simulations using the CTD code. Future fusion-power machines will be operated in advanced tokamak scenarios, where they deliberately avoid the appearance of low m/n neoclassical tearing modes and sawteeth instabilities keeping the central safety factor well above unity. Therefore,

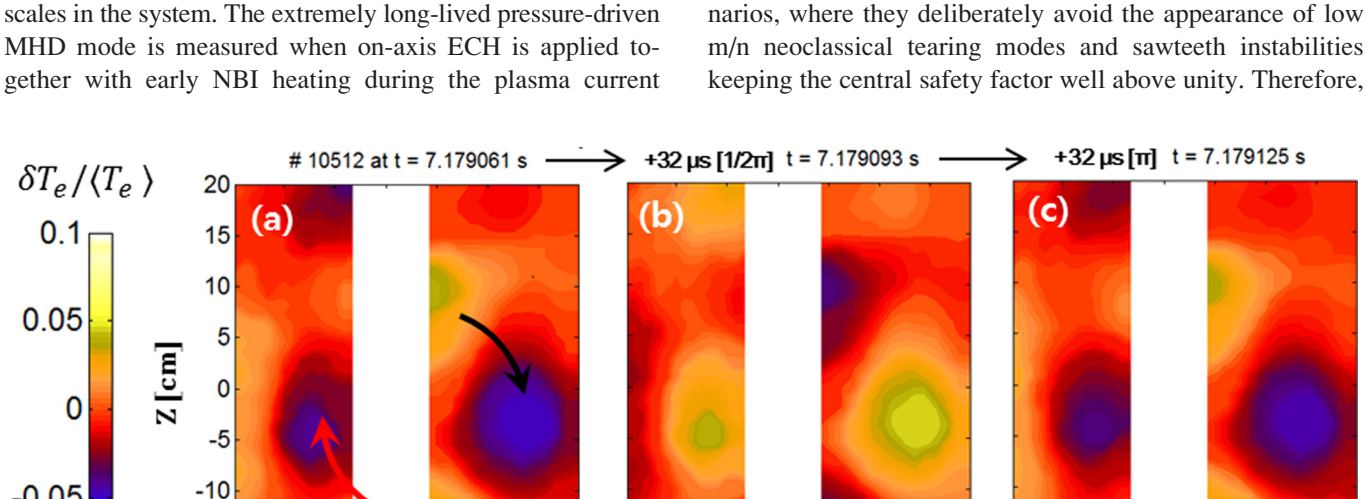

FIG. 8. Measured 2-D $\delta T_e/\langle T_e\rangle$ images by ECEI diagnostic. The arrows indicate the 2/1 mode rotation direction.

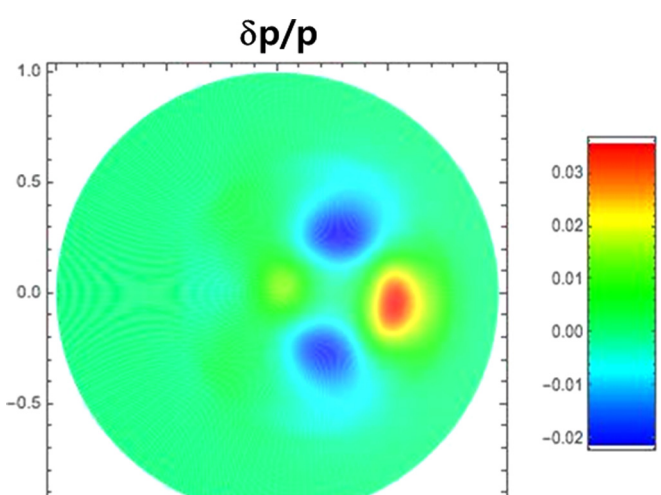

FIG. 9. Simulated pressure-driven mode. The nonlinear pressure perturbation δp calculated with the CTD code shows a strong ballooning character and is remarkably close to the measured ECEI image.

it is important to understand extremely long-lived pressure-driven mode reported in this experiment, since it will provide an essential contribution to core confinement and stability in steady-state burning plasma devices such as ITER and DEMO.

ACKNOWLEDGMENTS

The authors would like to acknowledge the KSTAR Team. This work was supported by the Korea Ministry of Science, ICT, and Future Planning under the KSTAR project contracts.

[1]A. Weller, A. D. Cheetham, A. W. Edwards, R. D. Gill, A. Gondhalekar, R. S. Granetz, J. Snipes, and J. A. Wesson, Phys. Rev. Lett. **59**, 2303 (1987).
[2]W. A. Cooper, J. P. Graves, A. Pochelon, O. Sauter, and L. Villard, Phys. Rev. Lett. **105**, 035003 (2010).
[3]W. A. Cooper, J. P. Graves, and O. Sauter, Nucl. Fusion **51**, 072002 (2011).
[4]J. A. Wesson, Plasma Phys. Controlled Fusion **28**, 243 (1986).
[5]A. Y. Aydemir, Phys. Rev. Lett. **59**, 649 (1987).
[6]F. L. Waelbroeck, Phys. Fluids B **1**, 499 (1989).
[7]L. Delgado-Aparicio, L. Sugiyama, R. Granetz, D. A. Gates, J. E. Rice, M. L. Reinke, M. Bitter, E. Fredrickson, C. Gao, M. Greenwald *et al.*, Phys. Rev. Lett. **110**, 065006 (2013).
[8]I. T. Chapman, M.-D. Hua, S. D. Pinches, R. J. Akers, A. R. Field, J. P. Graves, C. A. Michael, and MAST Team, Nucl. Fusion **50**, 045007 (2010).
[9]W. Deng, Y. Liu, X.-Q. Wang, W. Chen, Y.-B. Dong, S. Ohdach, X.-Q. Ji, Y. Shen, J.-Y. Cao, Z. Jun *et al.*, Nucl. Fusion **54**, 013010 (2014).
[10]J. G. Kwak, Y. K. Oh, H. L. Yang, K. R. Park, Y. S. Kim, W. C. Kim, J. Y. Kim, S. G. Lee, H. K. Na, M. Kwon *et al.*, Nucl. Fusion **53**, 104005 (2013).
[11]J. A. Snipes, D. J. Cambell, P. S. Haynes, T. C. Hender, M. Hugon, P. J. Lomas, N. J. L. Cardozo, M. F. F. Nave, and F. C. Schuller, Nucl. Fusion **28**, 1085 (1988).
[12]M. F. F. Nave and J. A. Wesson, Nucl. Fusion **30**, 2575 (1990).
[13]R. Fitzpatrick, Nucl. Fusion **33**, 1049 (1993).
[14]E. J. Strait, T. S. Taylor, A. D. Turnbull, J. R. Ferron, L. L. Lao, B. Rice, O. Sauter, S. J. Thompson, and D. Wróblewski, Phys. Rev. Lett. **74**, 2483 (1995).
[15]C. F. Figarella, S. Benkadda, P. Beyer, X. Garbet, and I. Voitsekhovitch, Phys. Rev. Lett. **90**, 015002 (2003).
[16]J. Seol, S. G. Lee, B. H. Park, H. H. Lee, L. Terzolo, K. C. Shaing, K. I. You, G. S. Yun, C. C. Kim, K. D. Lee *et al.*, Phys. Rev. Lett. **109**, 195003 (2012).
[17]S. C. Jardin, N. Ferraro, and I. Krebs, Phys. Rev. Lett. **115**, 215001 (2015).
[18]M. S. Chu, D. P. Brennan, V. S. Chan, M. Choi, R. J. Jayakumar, L. L. Lao, R. Nazikian, P. A. Politzer, H. E. St. John *et al.*, Nucl. Fusion **47**, 434 (2007).
[19]T. A. Casper, R. J. Jayakumar, S. L. Allen, C. T. Holcomb, L. L. LoDestro, M. A. Makowski, L. D. Pearlstein, H. L. Berk, C. M. Greenfield, T. C. Luce *et al.*, Nucl. Fusion **47**, 825 (2007).
[20]S. G. Lee, J. G. Bak, U. W. Nam, M. K. Moon, Y. Shi, M. Bitter, and K. Hill, Rev. Sci. Instrum. **81**, 10E506 (2010).
[21]R. V. Budny, M. G. Bell, H. Biglari, M. Bitter, C. E. Bush, C. Z. Cheng, E. D. Fredrickson, B. Grek., K. W. Hill, and H. Hsuan *et* al, Nucl. Fusion **32**, 429 (1992).
[22]L. L. Lao, J. R. Ferron, R. J. Groebner, W. Howl, H. St. Hohn, E. J. Strait, and T. S. Taylor, Nucl. Fusion **30**, 1035 (1990).
[23]G. S. Yun, W. Lee, M. J. Choi, J. B. Kim, H. K. Park, C. W. Domier, B. Tobias, T. Liang, X. Kong, N. C. Luhmann, Jr., and A. J. H. Donne, Rev. Sci. Instrum. **81**, 10D930 (2010).
[24]S. G. Lee, H. H. Lee, W. H. Ko, J. W. Yoo, and KSTAR Team, Fusion Sci. Technol. **69**, 555 (2016).
[25]I. G. Classen, E. Westerhof, C. W. Domier, A. J. H. Donne, R. J. E. Jaspers, N. C. Luhmann, Jr., H. K. Park, M. J. van de Pol, G. W. Spakman, M. W. Jakhbowski, and TEXTOR Team, Phys. Rev. Lett. **98**, 035001 (2007).
[26]M. J. Choi, G. S. Yun, W. C. Lee, H. K. Park, Y. S. Park, S. A. Sabbagh, K. J. Gibson, C. Bowman, C. W. Domier, N. C. Luhmann, Jr. *et al.*, Nucl. Fusion **54**, 083010 (2014).
[27]A. Y. Aydemir, J. Y. Kim, B. H. Park, and J. Seol, Phys. Plasmas **22**, 032304 (2015).